RESEARCH

Effective lifetime of Ni laser induced fluorescence excited at 336.9 nm during spark plug discharge

Ruike Bi[1] · Kailun Zhang[1] · Andreas Ehn[1] · Mattias Richter[1]

Abstract

In this study, the laser induced fluorescence lifetime of Ni atoms in ambient air with presence of a plasma discharge was measured for the first time. Free Ni atoms were generated in air at a pressure of 1 bar by spark plug discharges driven by an inductive coil. The Ni atoms were excited at the 336.957 nm absorption line by a 336.96 nm, 90 ps laser pulse and the resulting temporally resolved decaying fluorescence signals were captured by a PMT. An effective fluorescence lifetime of about 1.1 ns was observed for the fluorescence signal within a 7.4 nm detection window centered at 345 nm. Further analysis also revealed that the lifetime of the transition showed statistically insignificant change throughout the duration of the discharge. The peak intensity of the fluorescence signal was found to be proportional to the integrated signal intensities. This in turn suggests that the integrated fluorescence signals in the aforementioned spectral region are proportional to the population density of ground state Ni atoms in the detection volume. The number density of free Ni atoms in the spark gap was measured over time during the plasma discharge, showing an accumulating trend in the beginning phase of the discharge followed by a slow decrease until the termination.

1 Introduction

Spark plugs are an essential component in a spark-ignited engine and play a vital role in the performance of the engine. This means that spark plugs operate in harsh environments involving elevated temperature and high pressure. Additionally, the spark discharge produces high temperature plasma and high energy ion and electron flows, which causes erosion of the spark electrodes [1]. The spark plug electrode erosion leads to an increased gap between said electrodes and in the required ignition voltage, which eventually will cause misfires in the engine [2–4]. Current spark plug lifetimes are typically 1000–4000 h, which is shorter than the over 8000 h desired by the industry, causing extra down time and cost for changing of the spark plugs [4]. Spark plug electrode wear is accentuated in hydrogen fueled spark ignited internal combustion engines (H2 SI-ICE). The development of such zero emission engines currently attracts significant attention in the effort to mitigate the climate crisis.

Therefore, it is highly desirable for the industry to understand and control electrode erosion in spark plugs in order to reduce the total cost of ownership and make H2 SI-ICE a viable alternative to other zero emission solutions such as battery electric and fuel cell drivelines.

An optical diagnostic approach was proposed to study the electrode erosion process in spark plugs, which is based on spontaneous emission of Ni atoms in the spark gap [5]. A spectral region between the nitrogen emission bands at 337.0 nm and 353.6 nm was found to be free of emission from the discharge and cover multiple emission lines of Ni atoms. Such findings provide an approach for monitoring the erosion dynamics of the spark plug electrode during the discharge, based on which information new discharge driving strategies can be proposed for minimizing electrode wear while maintaining the ignitability. Earlier unpublished work revealed that excitation of Ni atoms to the $3d^9(^2D)4p^\circ$ $J = 3$ state at 336.957 nm can induce LIF with an optimal signal-to-noise ratio (SNR) in the desired detection window. This excitation wavelength and detection window enables 2D Ni atom LIF in the spark gap. 2D LIF is valuable in that it can provide information on the spatial distribution of Ni atom plumes in addition to the temporal erosion dynamics. However, it is the Ni atom number density which needs to be measured for increased understanding on

✉ Ruike Bi
  ruike.bi@fysik.lu.se

1   Division of Combustion Physics, Department of Physics, Lund University, Box 118, Lund 22100, Sweden

how the erosion of the spark plug electrodes are developing. To correlate the measured Ni atomic LIF signal intensity to Ni atom number density, one needs knowledge in the lifetime of the fluorescence signal and how it changes across the duration of the spark discharge [6, 7].

Previously, some work has been done for detection of Ni atoms present in furnaces or during carbon nanotube formation using excitation wavelengths at sub-300 nm [8–11], but no study was made on properties of Ni atomic LIF using the excitation scheme studied in this work. Lifetime measurements of some Ni I transitions have been performed earlier [12–15]. However, in these experiments, the measurements were done when the free Ni atoms are at a stable state with a carrier gas of Ar at pressures ranging from 0.4 to 15 Torr. In the present work, lifetime of Ni atomic transitions was measured in ambient air. Furthermore, the lifetime measurement was performed with the presence of the spark discharge, therefore taking into consideration the interaction between the Ni atoms and the discharge plasma. The results in the current study provide added information on Ni fluorescence lifetime and provide support for further application of planar LIF detection of Ni atom number density during a spark discharge.

2 Lifetime of a decaying signal affecting the integrated fluorescence intensity

Assuming that a given fluorescence signal that decays exponentially with a lifetime of τ is being imaged by an integrating detector. The expression for the decaying signal can be written as:

$$f(t) = I_0 e^{-\frac{t}{\tau}}, \tag{1}$$

where $f(t)$ is the fluorescence intensity at a given time t $(t \geq 0)$, and I_0 is the peak fluorescence intensity. A simple model of the detector assumes a gate width T and 0 s

rise and fall time, which means that the gate function of the detector $G(t)$ can be written in the form of a top-hat function:

$$G(t) = \begin{cases} 1, & 0 \leq t \leq T \\ 0. otherwise \end{cases} \tag{2}$$

.The integrated fluorescence intensity captured by the detector $s(T)$ takes the form:

$$\begin{aligned} s(T) &= k \int_0^\infty G(t) * I_0 e^{-\frac{t}{\tau}} dt \\ &= kI_0\tau \left(1 - e^{-\frac{T}{\tau}}\right), \end{aligned} \tag{3}$$

where k is a constant representing the optical collection efficiency and quantum yield of the detector. From Eq. (3), it can be seen that when detected by an integrating detector using a fixed gate width T, the integrated fluorescence intensity is controlled by two quantities, the peak fluorescence intensity I_0, which is proportional to the number density of the detected species, and the lifetime of the decay, τ. An illustration of the above discussion is made in Fig. 1, where Fig. 1 (a) shows various decay curves with different lifetimes, and Fig. 1 (b) showing the integrated intensity as a function of the lifetime of the decay. Therefore, prior knowledge of the lifetime of a fluorescence signal must be acquired to derive information on number density of the fluorescing species based on a camera measurement.

3 Experimental setup

A schematic drawing of the experimental setup is shown in Fig. 2 (a) and a zoomed-in view on the electrodes is shown in Fig. 2 (b). The spark discharge was generated using a test rig developed by Swedish Electro Magnets AB. In the test rig, the central electrodes of two conventional spark plugs, whose ground electrodes had been removed, were used for discharge generation. One of the electrodes was negatively

Fig. 1 (**a**): Decay curves with the same peak intensity but different lifetimes. (**b**): Integrated intensity using a top-hat shaped gate function between 0 and 3 ns as a function of lifetime
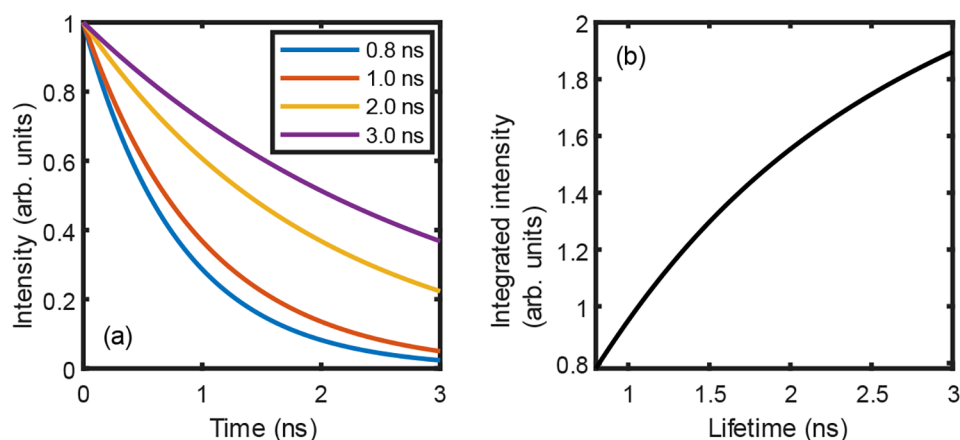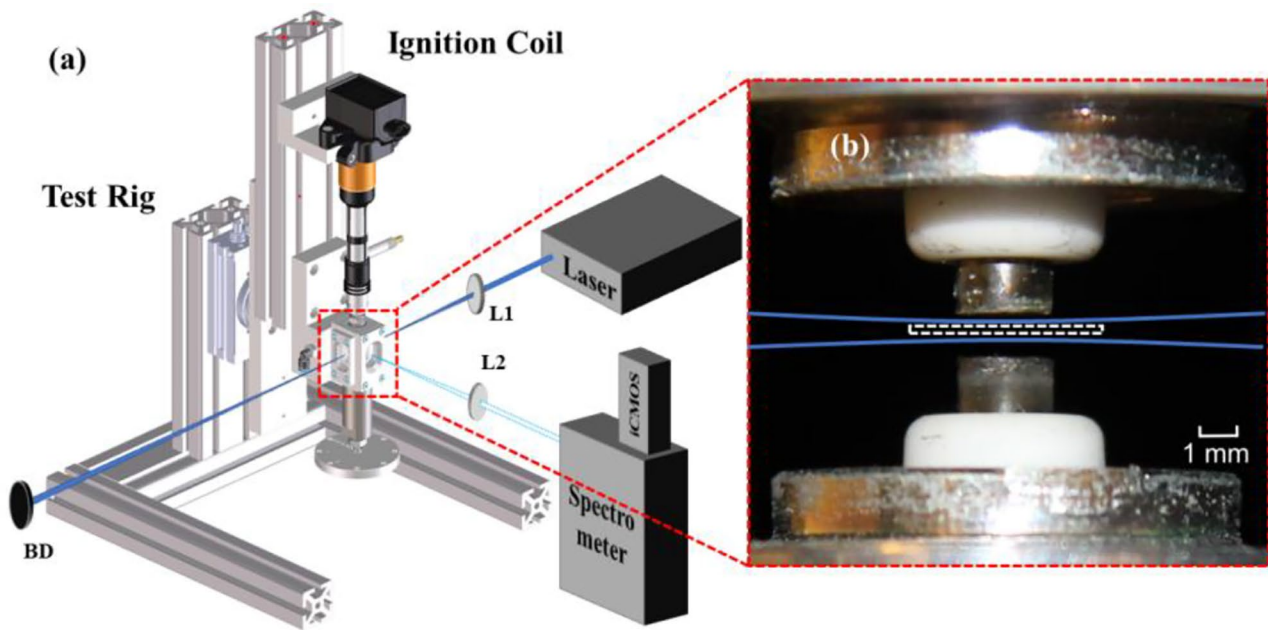
Fig. 2 A schematic drawing of the experimental setup. (**a**): overview of the setup. (**b**): zoomed-in view on the spark electrodes, white rectangle indicating the detection region of the entrance slit and blue curve the path of the excitation laser. L1, L2: positive lenses, BD: beam dump

driven by an inductive coil to serve as the cathode, and the other was grounded, serving as the anode. The distance between the two electrodes was set to be 1 mm. In the presented study, a coil charging time of 3 ms was used to generate a discharge vertically between the two electrodes that has a plasma channel with a diameter less than 0.1 mm, lasting for about 3.5 ms long. The excitation source was a tunable pico-second laser system (Ekspla UltraFlux FT405). The 400 µJ, 90 ps laser pulse with a bandwidth of approximately 10 cm^{-1} centered at 336.96 nm, which was generated by doubling the output of an optical parametric oscillator (OPO) pumped by the third harmonic of the laser at 355 nm, was sent into the spark gap with varied delay relative to the initiation of the spark discharge to excite the Ni atoms in the spark gap from the ground state to the $3d^9(^2D)4p^\circ$ $J = 3$ state [16]. The delay was scanned from 50 µs to 3500 µs with a step size of 50 µs. The resulting fluorescence signals were focused by a UV objective lens (B. Halle 100 mm f2, L2) into a spectrometer (Princeton Instrument Acton SpectraPro 2300i) equipped with a 1200 grooves/mm grating whose blaze wavelength was 300 nm, and the spectrometer's entrance slit was set perpendicular to the plasma channel, as indicated by the dashed white rectangle in Fig. 2 (b). The LIF spectrum was captured by an ICMOS camera (Andor iStar intensified sCMOS) at the exit of the spectrometer. In the PMT measurements, an exit slit was placed at the exit of the spectrometer instead of the camera, the width of which was set to its maximum at 3 mm, corresponding to a spectral window with approximately 7.4 nm width. The

angle of the grating was tuned so that the detection window was centered at 344.5 nm. The spectrally filtered signal was sent into a Hamamatsu R5916U-50 MCP-PMT with a fall time of 700 ps, and the output is registered by an oscilloscope (Teledyne LeCroy WavePro 604HD 6 GHz 20 Gs/s). For each delay time relative to breakdown, 500 temporally resolved LIF signals were averaged to form one measurement. The resulting PMT signal traces were later processed and analyzed in MATLAB. PMT signals were also taken at 300 µs after breakdown when the excitation wavelength was tuned to 336.96 ± 0.1 nm.

To correlate the integrated fluorescence intensity to the peak fluorescence intensity, and hence the population density of excited Ni atoms in the spark gap, measurement of a realistic camera gate function was also performed. To measure the gate function, the same ICMOS camera as the one used in the spectroscopy measurement was used on the exit end of the spectrometer. The Rayleigh scattered light of the 90 ps, 336.94 nm laser pulse was captured by the camera with a set gate width of 2.1 ns. Intensity of the 336.94 nm laser line captured by the camera was plotted as a function of delay between laser pulse and camera gate, forming the mapped gate function. Following the smoothing and normalization of the function, a linear interpolation was also applied to match the scanning step size (0.1 ns) with the temporal resolution of the oscilloscope (0.05 ns). The simulated integrated fluorescence intensity $S_{integrated}$ can be denoted as:

$$S_{integrated} = \int_0^{T\infty} G(t) * s(t)\, dt, \tag{4}$$

where $G(t)$ is the interpolated gate function and $s(t)$ is the PMT signal curve.

4 Results and discussion

Ni was chosen as the main metal to study because it is one of the most used materials for spark plug electrode production, which can be representative of the erosion characteristics during discharges. A LIF spectrum with excitation at 336.96 nm is shown in Fig. 3 (a), along with the detection window for the PMT measurement shown in red. The observed fluorescence lines were compared with the atomic line data in the NIST database [16] and found to agree with that of Ni atoms. To eliminate the possibility of Ni ions contributing to the spectra, both the emission lines and the absorption line have been checked against the ionized Ni data. Ni ions don't show absorption at the excitation wavelength, and the wavelengths of the observed emission lines

don't agree with that from the Ni ions. The electrodes being tested in the current experiment consist of $\geq 94\%$ Ni. Other metals such as Fe, Cr or Mo can be found in the nickel alloy used in the sample in the current experiment, but they are only present in trace amounts, therefore not able to produce signal intensity as a significant level. These metals also have no potential transitions that can be excited by the laser wavelength used in the current study. Therefore, confirmation can be made that the observed LIF spectrum is only from Ni atoms.

Part of the Ni atom energy diagram is illustrated in Fig. 3 (b) and the identified transitions in Fig. 3 (a) are drawn, the excitation in solid line and the fluorescence in dotted lines, among which the ones included in the detection window are drawn in red. It is worth noting that the configuration of the upper level, $3d^9(^2D)4p$, has strong interactions with configurations $3d^84s4p$ and $3d^95p$, therefore drastically complicating the current excitation scheme [17–19]. Specifically, the two largest components of the eigenvector of $3d^9(^2D)4p^\circ$ $J = 3$ are $3d^9(^2D)4p\,^3D^\circ$ and $3d^8(^3F)4s4p(^3P^\circ)\,^5F^\circ$, which takes up 60% combined. In addition, the observation of fluorescence lines originating

Fig. 3 (**a**): Ni atom LIF spectrum excited at 336.96 nm, with the observed fluorescence peaks numbered; (**b**): Ni atom energy level diagram and observed transitions in (**a**), transitions that are included in the detection window for PMT measurement marked in red
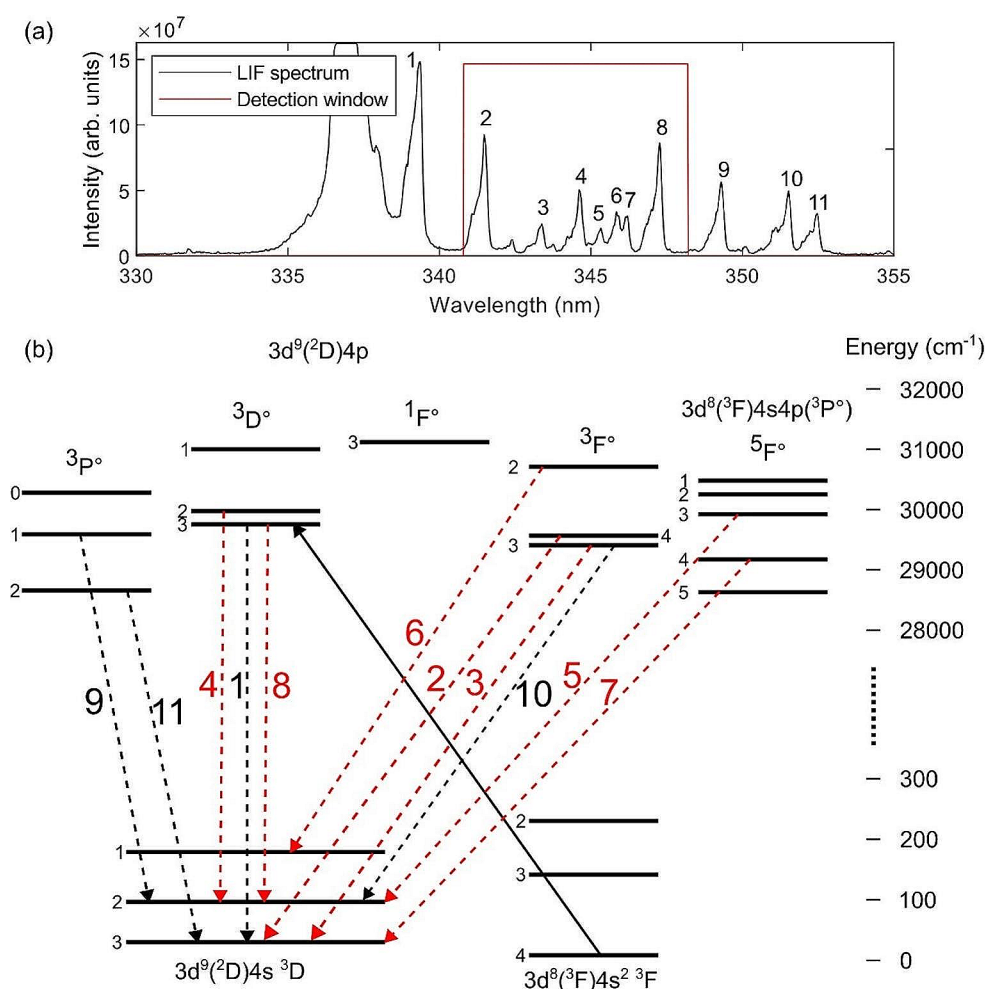
from the $3d^9(^2D)4p\,^3P^\circ$ and $^3F^\circ$ states indicates the occurrence of collisional relaxation from the excited state.

To confirm the nature of the signal captured by the PMT, the excitation laser was tuned to 336.86, 336.96 and 337.06 nm, and corresponding PMT signal traces were recorded, as shown in Fig. 4. The peak intensity recorded with the laser tuned to 336.96 nm (Fig. 4 (b)) was more than double of what was recorded with excitation at 336.86 nm (Fig. 4 (a)) and 337.06 nm (Fig. 4 (b)). The signal rise when excited by the 336.96 nm laser pulse provided confirmation that the signal captured by the PMT is resonant signal induced by the laser. The 10 cm^{-1} bandwidth of the excitation laser corresponds to a full width at half maximum (FWHM) of about 0.11 nm and 0.1 nm was the smallest tunning step size of the OPO. Literature shows that the center of the absorption profile located at 336.957 nm [20, 21], which means the excitation laser has the most overlap with the absorption profile when tuned to 336.96 nm. When tuned away by ±0.1 nm, an overlap between the laser spectral profile and the atomic absorption profile still exists but is smaller compared to the 336.96 nm case. Therefore, considerable levels of fluorescence can still be observed in both cases, but at a lower intensity. It was also observed that a higher peak signal intensity was captured when excited at 336.86 nm (Fig. 4 (a)) compared to when excited at 337.06 nm (Fig. 4 (c)). This can be explained by the fact that the central wavelength of the absorption profile lies closer to the central wavelength when excitation wavelength was tuned to -0.1 nm, thus having a larger overlap with the laser spectral profile. Also observed in Fig. 4 is the presence of a secondary peak at about 5 ns. This secondary peak can be seen in all the PMT traces recorded throughout this experiment, whose intensity does not scale with the peak intensity of the LIF signal. We therefore presume that this peak is a laser-induced background arising from excitation laser

pulse scattered in the spectrometer and should be avoided in the data analysis.

Examples of signal traces captured by the PMT are shown in Fig. 5 (a) and (b). In Fig. 5 (a), where the signal was taken at 150 μs after breakdown, a peak signal level of 0.022 V is reached. In this case, most of the signal comes from fluorescence emitted by the excited Ni atoms. In Fig. 5 (b), where the signal was taken at 3300 μs after breakdown, the peak signal level was less than 0.005, which indicates a dramatic drop in Ni LIF intensity towards the end of the spark duration.

Based on the observation above, the signal between 0.65 ns and 2.90 ns was selected for the exponential fitting. This region was selected to avoid the very peak of the LIF decay, so that the impact on the fitting from variation in excitation energy can be minimized, and to avoid the secondary peak, the cause of which has been discussed. The intensity of the selected region was normalized by dividing with its maximum. The data was first shifted in time so that the first data point starts from 0, and then normalized temporally by dividing with the width of the selected time window, t_{tot}. Logarithmic fit was then performed using the following model,

$$f(x) = ae^{(-\frac{x}{b})}, \tag{5}$$

where a and b are fitting parameters. The lifetime of the decay in normalized time would then be expressed as:

$$\tau = b*t_{tot}. \tag{6}$$

In Fig. 5 (c) and (d), the exponential fit of the two decays at 150 μs and 3300 μs after breakdown, respectively, are plotted. At 150 μs after breakdown when the LIF signal is high, the decay curve can be very well represented by the exponential fit. In this case, the lifetime calculated for the
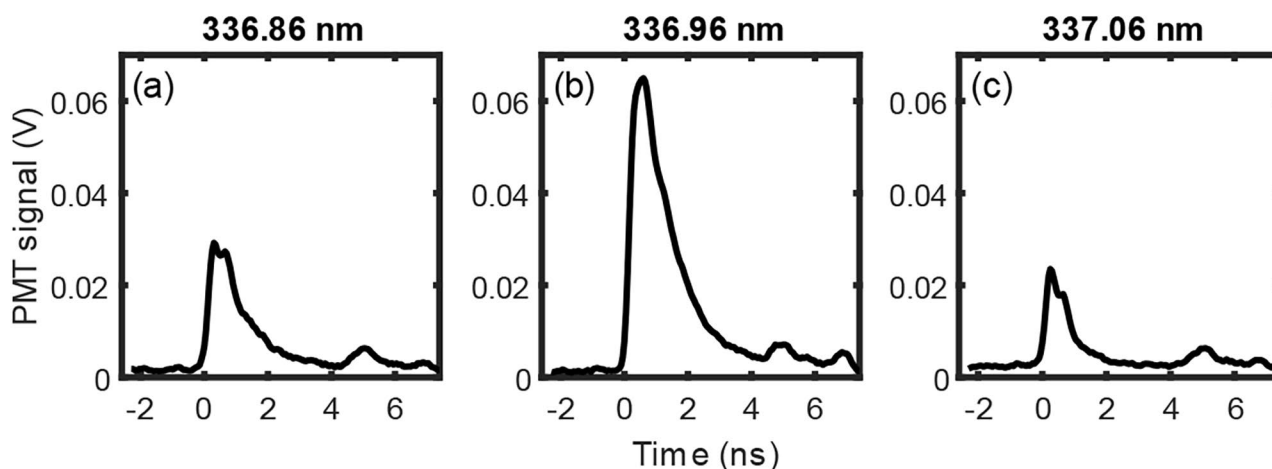

Fig. 4 PMT signal at 300 μs after breakdown excited by different wavelength. (**a**): 336.86 nm, (**b**): 336.96 nm and (**c**):337.06 nm
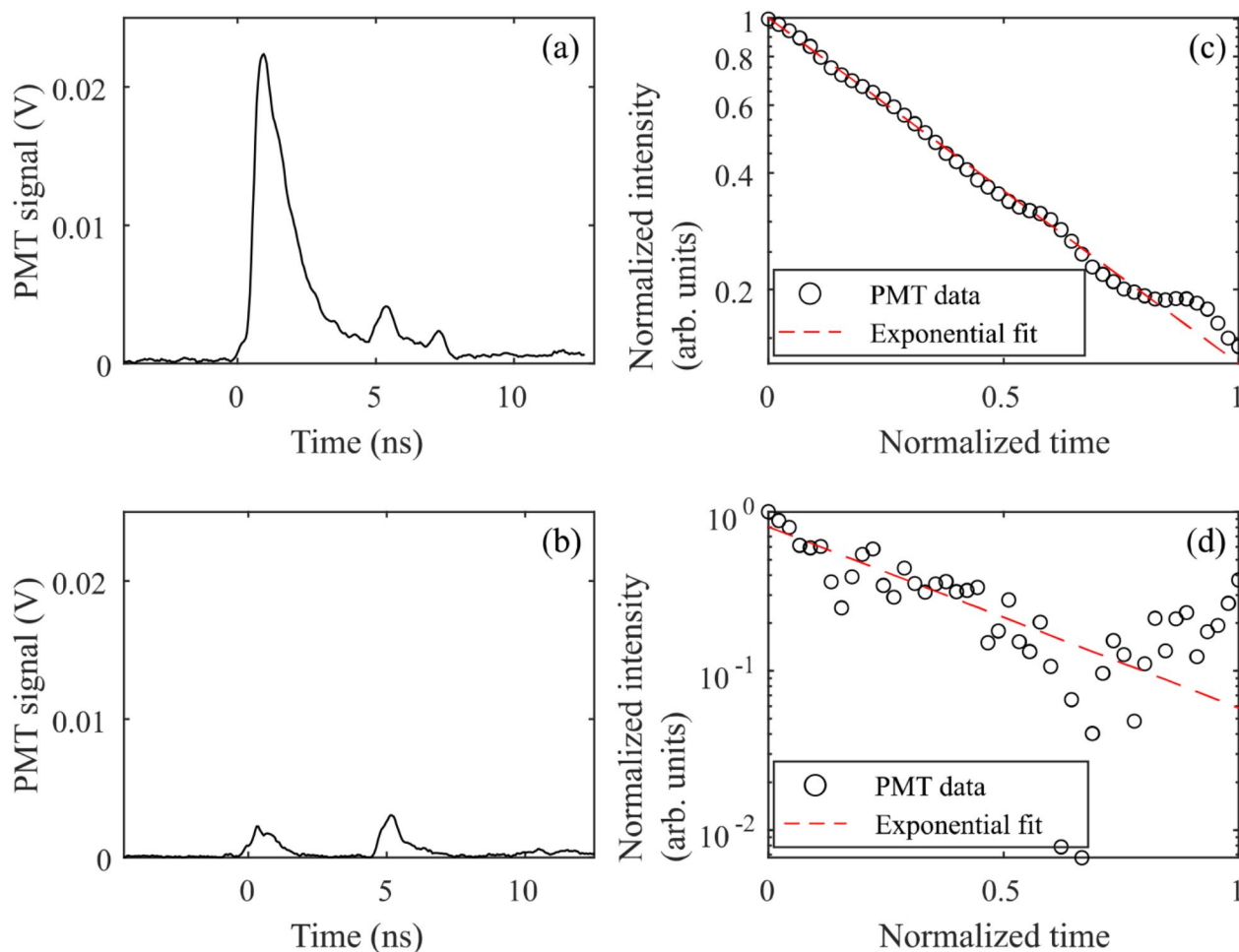
Fig. 5 (**a**), (**b**) Example signal traces captured by the PMT at 150 μs and 3300 μs after the breakdown, respectively; (**c**), (**d**) exponential fit of the decay at 150μs and 3300 μs after the breakdown, respectively
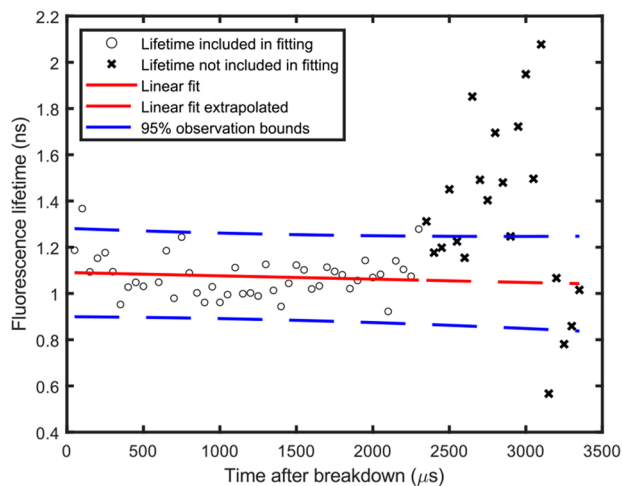

Fig. 6 Measured Ni LIF lifetime in the spark discharge and fitted lifetime

LIF signals is about 1.1 ns. In Fig. 5 (d), however, the quality of the fitting became poor as the intensity dropped. This issue persists in all the measurements in the later stage of the spark discharge.

In Fig. 6, all measured Ni LIF lifetimes in the experiment are plotted in a scatter plot. A linear fit was made to the data points to provide an estimation of the Ni fluorescence lifetime at a given time after breakdown. Due to the above-mentioned fitting quality issue, only the data acquired before 2300 μs after breakdown were used in the fitting. The lifetime of Ni LIF after 2300 μs is estimated by extrapolating the linear fit and plotted as the red dashed line in Fig. 6. From the initiation of the discharge to the end, the LIF lifetime measurements scatter evenly around the linear fitted line with a slope of -1.43×10^{-5} ns/μs. According to the fitted model, the predicted lifetime decreases by around 0.043 ns from breakdown to the end of the discharge, which is about 4% of the 1.1 ns lifetime. The 95% prediction bounds, calculated using MATLAB's predint function, are
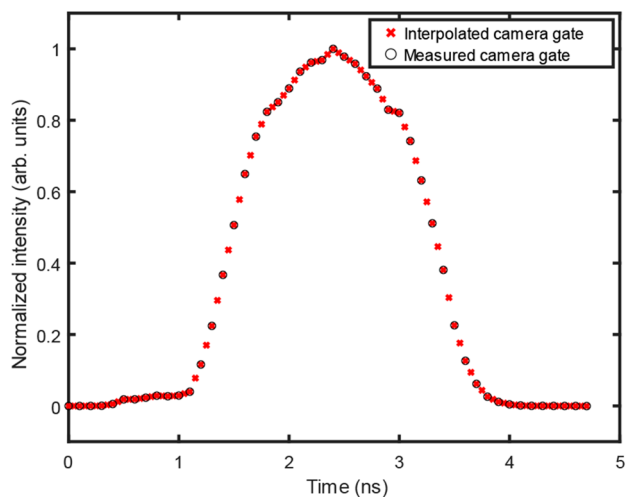
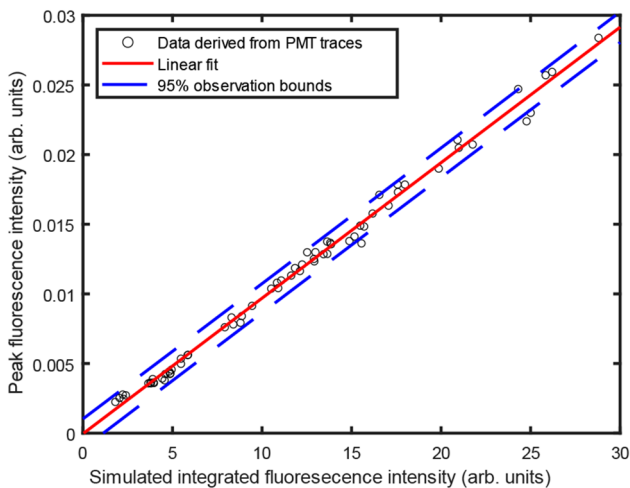Fig. 7 Measured camera gate function before and after interpolation

Fig. 8 Peak fluorescence intensity plotted as a function of simulated integrated fluorescence intensity
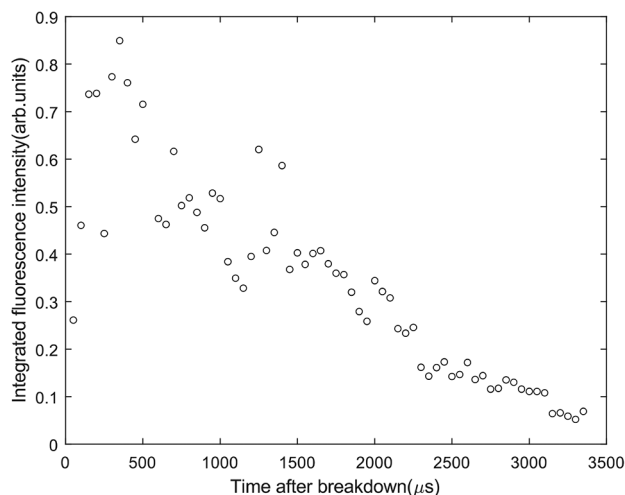

Fig. 9 Change in integrated fluorescence intensity over time after breakdown

In Fig. 8, each point represents one decay captured by the PMT, with the peak fluorescence intensity on the y-axis. The simulated integrated fluorescence intensity captured by an Andor ICMOS camera, calculated by Eq. (4) with $G(t)$ as the gate function, is on the x-axis. A linear fit was performed and plotted as the red line, together with the 95% observation bounds plotted as the blue dashed lines. The peak fluorescence intensity is proportional to the simulated integrated fluorescence intensity as indicated by the line of best fit crosses the origin of the plot in Fig. 8. Since the peak fluorescence intensity is proportional to the number density of Ni atoms, the integrated fluorescence intensity can be considered proportional to the Ni atom number density. This means that the LIF signal captured by an integrating detector, for example a camera, at different times after the initiation of the discharge can be taken as proportional to the number density of Ni atoms in the detection volume.

While the calculation of the simulated fluorescence intensity presented in Fig. 8 has been made based on a specific gate function, the conclusion drawn from the figure holds true when the integration is done by a different gate, supposing that the gate is wide enough and the majority of the fluorescence signal gets captured by it. However, getting the knowledge of the gate function is always beneficial, as one can find out the rise and fall time of the camera, therefore synchronizing the gate for maximized fluorescence signal level with the lowest possible background.

In Fig. 9, the simulated fluorescence intensity is plotted against time after initiation of the discharge. From the previous discussions, it has been established that throughout the life of the discharge, the integrated fluorescence intensity is proportional to the population of Ni atoms. Therefore, Fig. 9 can serve as a qualitative indication of the development of

from around 0.9 ns to 1.3 ns throughout the duration of the discharge and are much larger than the change predicted by the fitted model. Therefore, the change in lifetime across the duration of the discharge is not statistically significant. As a result, the lifetime of Ni fluorescence can be considered to stay constant throughout the duration of the discharge at about 1.1 ns. In a previous work of Bergeson and Lawler, a lifetime of 10.4 ns was reported for the Ni 341.6 nm emission in an environment of 0.4 Torr of Ar [14, 22]. The much shorter decay time measured in the current work is due to the more significant collisional quenching at ambient pressure.

The measured gate function and the interpolated function $G(t)$ are plotted in Fig. 7. The original gate function is denoted as black circles and the interpolated gate function as red crosses. Figure 8 illustrates how the Ni atom population is related to the captured integrated fluorescence intensity.

the Ni population in the spark gap. A rapid accumulation of Ni atoms happens in the early phase of the discharge, namely from discharge initiation until around 350 μs afterwards. After the peak at approximately 350 μs after discharge initiation, the Ni population starts to drop, suggesting a decreased generation rate of free Ni atoms. This trend of integrated fluorescence intensity and thus Ni population is in agreement with the spontaneous emission intensity trends reported in a previous work [5].

It should be emphasized that the measured lifetime in the presented work is an effective lifetime of the decaying of the fluorescence signal that falls in the detection window, which reflects the combined lifetime of both the excited state and the lower state and may be subject to changes depending on the excitation scheme used. The presented study is also limited in that the lifetime measurements has been performed at 1 bar, but the working environment of the spark plug in an engine is vastly different, both in pressure and gas composition. In engine conditions, the additional quenching due to elevated pressure will cause further shortening of the lifetime, but such effects are expected to be uniform across the spark gap, therefore not diminishing the proportional correlation between the integrated fluorescence intensity and the Ni atom number density established by the current study, which means that 2D LIF studies on Ni atom distribution is still valid in engine conditions. The current proposed excitation scheme is only valid for Ni and the results on electrode erosion will only be applicable to metals that share similar physical properties as Ni. Additional excitation studies must be carried out for the study of erosion characteristics of metals such as Ir or W due to their differences in photophysical properties.

5 Conclusions

The combined Ni LIF lifetime was derived in air at 1 bar, using a picosecond laser pulse at 336.96 nm as the excitation source. The effective fluorescence lifetime in a detection window centered at about 354 nm and with a width of approximately 7.4 nm was measured to be about 1.1 ns throughout the duration of the discharge. A linear fit of the lifetime data provided a 95% prediction bound in the lifetime of 0.9 ns to 1.3 ns.

The relationship between a simulated integrated fluorescence intensity using a measured camera gate function and the peak fluorescence intensity was also studied. Within the whole duration of the discharge, the simulated integrated fluorescence intensity was shown to be proportional to the peak fluorescence intensity. Therefore, when detected with by a camera with a fixed gate width, the intensity of the LIF signal studied in the present experiment is proportional

to the population of excited Ni atoms in the corresponding area. Based on these results, the change in Ni atom number density over time after discharge initiation was qualitatively plotted and the results agree with a previous study [5]. This conclusion supports future studies on the 2D distribution of Ni atom distribution in the spark gap.

Declarations

Competing interests The authors declare no competing interests.

References

1. R. Maly, Spark Ignition: its physics and effect on the Internal Combustion Engine, *Fuel Economy: In Road Vehicles Powered by Spark Ignition Engines* (Springer US, Boston, MA 1984), 91–148
2. S. Javan, S.S. Alaviyoun, S.V. Hosseini, F. Ommi, J. Mech. Sci. Technol. **28**(3), 1089–1097 (2014)
3. S. Javan, S. Hosseini, S. Alaviyoun, F. Ommi, Engine Res. **26**(26), 31–39 (2012)
4. H.T. Lin, M.P. Brady, R.K. Richards, D.M. Layton, Wear. **259**(7–12), 1063–1067 (2005)

5. R. Bi, Time-Resolved Diagnostic of Electrode Erosion in Spark Plugs (Lund University 2019), http://lup.lub.lu.se/student-papers/record/8981220

6. J. R. Lakowicz, quenching of fluorescence, in *Principles of Fluorescence Spectroscopy* (Springer US, Boston, MA 1983), pp 257–301

7. A. C. Eckbreth, Laser-induced fluoresecence (LIF), in *Laser Diagnostics for Combustion Temperature and Species* (Overseas Publishers Assosiation Amsterdam B.V., Netherlands 1996), pp 381–466

8. M. Cau, N. Dorval, B. Attal-Trétout, J.L. Cochon, A. Foutel-Richard, A. Loiseau, V. Krüger, M. Tsurikov, C.D. Scott, PhRvB **81**(16), 165416 (2010)

9. N. Dorval, A. Foutel-Richard, M. Cau, A. Loiseau, B. Attal-Trétout, J.L. Cochon, D. Pigache, P. Bouchardy, V. Krüger, K.P. Geigle, J. Nanosci. Nanotechnol. **4**(4), 450–462 (2004)

10. A. Marunkov, N. Chekalin, J. Enger, O. Axner, Spectrochimica Acta Part. B: at. Spectrosc. **49**(12), 1385–1410 (1994)

11. G. De Boer, S. Arepalli, W. Holmes, P. Nikolaev, C. Range, C. Scott, J. Appl. Phys. **89**(10), 5760–5768 (2001)

12. D. Blackwell, A. Booth, A. Petford, J. Laming, Mon Not R Astron. Soc. **236**(2), 235–245 (1989)

13. J. Heldt, H. Figger, K. Siomos, H. Walther, Astron. Astrophys. **39**, 371 (1975)

14. S.D. Bergeson, J.E. Lawler, J. Opt. Soc. Am. B **10**(5), 4 (1993)

15. X. Shang, Q. Wang, F. Zhang, C. Wang, Z. Dai, J. Quant. Spectrosc. Radiat. Transf. **163**, 34–38 (2015)

16. A. Kramida, Y. Ralchenko, J. Reader, N.I.S.T.A.S.D. Team, NIST Atomic Spectra Database (ver. 5.11) [Online], Available: https://physics.nist.gov/asd National Institute of Standards and Technology, Gaithersburg, MD

17. C. Roth, ADNDT. **25**(2), 91–184 (1980)

18. C. Roth, A. Section, Phys. Chem. **74**(5), 715–722 (1970)

19. J. Ruczkowski, M. Elantkowska, J. Dembczyński, Mon Not R Astron. Soc. **464**(1), 1127–1136 (2016)

20. A. Doerr, M. Kock, J. Quant. Spectrosc. Radiat. Transf. **33**(4), 307–318 (1985)

21. M. Huber, R. Sandeman, Astron. Astrophys. **86**, 95–104 (1980)

22. T.R. O'Brian, M.E. Wickliffe, J.E. Lawler, W. Whaling, J.W. Brault, J. Opt. Soc. Am. B **8**(6), 6 (1991)